Engineering Science and Technology, an International Journal 59 (2024) 101873

Contents lists available at ScienceDirect

Engineering Science and Technology, an International Journal

journal homepage: www.elsevier.com/locate/jestch

Full Length Article

Design and real-time implementation of a sliding mode observer utilizing voltage signal injection and PLL for sensorless control of IPMSMs

Ertugrul Ates [a,c], Burak Tekgun [a,*], Gunyaz Ablay [a], Murat Barut [b]

[a] Electrical and Electronics Engineering Department, Abdullah Gul University, Kayseri 38080, Turkiye
[b] Electrical and Electronics Engineering Department, Niğde Omer Halisdemir University, Niğde 51240, Turkiye
[c] Computer Engineering Department, Niğde Omer Halisdemir University, Niğde 51240, Turkiye

ARTICLE INFO

Keywords:
Sensorless control
Signal injection
IPMSM
Sliding mode observer
PLL

ABSTRACT

In this study, a sliding mode observer (SMO) based on high-frequency (HF) voltage signal injection and a phase-locked loop (PLL) is proposed for estimating the extended electromotive force (EEMF), rotor position, and rotor velocity of an interior permanent magnet synchronous machine (IPMSM). This approach addresses real-time estimation challenges associated with standard SMO and PLL at very low speeds and standstill. A reliable and accurate sensorless speed control system for IPMSM is then developed and implemented in real time using the proposed SMO and PLL, covering a wide range of speeds, including low-speed and standstill conditions. The SMO effectively estimates the EEMF, while the PLL extracts the rotor velocity and position based on these estimates. Compared to conventional SMO and PLL methods, real-time results from an 8-pole, 0.4 kW IPMSM demonstrate the superior efficiency of the proposed system.

1. Introduction

Interior permanent magnet synchronous machines (IPMSM) are utilized in industry thanks to the features of high power factor, high efficiency, good dynamic performance, and high power density [1,2]. Today, the most advanced alternative current (AC) machines are controlled with the vector (field-oriented) control scheme for high dynamic performances. In this method, the rotor angle and stator excitation should be in sync, and thus a rotor position measurement is needed. To reduce the cost, maintenance, and reliability constraints of the mechanical position sensors, the position sensorless control method with a position/speed estimation algorithm is preferred to eliminate the mechanical detectors.

In the literature, the rotor speed/position estimation of IPMSM is currently performed by using both:

(i) the model based methods of either open loop estimators with the back electromotive force (back EMF)/the extended EMF (EEMF)/the active flux (AF) estimations [3–9] or closed loop state observers — with deterministic models of model reference adaptive system (MRAS) [10], the disturbance observer [11], flux observer [12], sliding-mode observer (SMO) [4] -with stochastic models of extended Kalman Filters [13–16], adaptive extended Kalman filter [17].

Those can be satisfactorily used at only medium- or high-speed sensorless operation of IPMSMs but their real time performances deteriorate at very low speeds (usually below 10% of the rated speed [4]) and fail at zero speed since the back EMF/EEMF becomes too small and/or the signal-to-noise-ratio caused by uncertainties and measurement noises increases. However, the rotor position of IPMSMs is detectable at standstill if stator current components (i_d and i_q) are not linearly dependent and are changing both magnitude and direction [8], which directly calls for or suggests the utilization of *HF signal injection* based approaches at zero speed (or nearly at zero speed).

(ii) the saliency tracking-based method of rotating (at stator stationary $\alpha\beta$-axes)/pulsating (at synchronous dq-axes) *signal injection* and fundamental pulse width modulation (PWM) *excitation* [7], which provide stable estimation performances at very low speed and standstill, but have to be utilized along with the model based observers/estimators for a full speed range sensorless operation of IPMSM as stated in [18] introducing a smooth transition between the saliency tracking-based method (starting algorithm) and the back-EMF based sensorless algorithm above a particular threshold speed. Thus, it can be concluded that the model based estimators or observers [7] are also needed for a sensorless control of IPMSMs in a vast range of speeds. Model-based approaches, such as the Luenberger observer, are known for their simplicity in design. However, they may struggle to accurately represent the behavior of IPMSM due to its nonlinear and strongly coupled nature, potentially leading to poor performance and instability in sensorless control systems [4]. On the other hand, Kalman filter

* Corresponding author.
E-mail addresses: ertugrul.ates@agu.edu.tr (E. Ates), burak.tekgun@agu.edu.tr (B. Tekgun), gunyaz.ablay@agu.edu.tr (G. Ablay), mbarut@ohu.edu.tr (M. Barut).

https://doi.org/10.1016/j.jestch.2024.101873
Received 30 May 2024; Received in revised form 1 October 2024; Accepted 13 October 2024
Available online 28 October 2024

methods adjust the observer gain matrix during each control cycle to strike a balance between model accuracy and sensor data. Despite their robustness, these methods are hindered by high computational complexity and difficulties in configuring the covariance matrices in real-world applications [17]. Among them, the SMO is one of the most useful closed loop observer for the position sensorless control of IPMSMs owing to its resilience against variations in machine parameters and disturbances together with its simple realizations [4]. In [19], the estimated EEMF terms ($\hat{e}_\alpha$ and $\hat{e}_\beta$) and stator currents in the $\alpha\beta$-axes are firstly obtained by the traditional sign-function-based full order SMO and then the estimations of rotor position and velocity are reached by the conventional PLL instead of using the arctangent function ($\hat{e}_\alpha$ / $\hat{e}_\beta$) which is sensitive to noise and harmonics and results in significant estimation errors as $\hat{e}_\beta$ passes zero when the EMF changes its polarity; Later, those estimations are performed by the improved full order SMO utilizing a piecewise power function in place of the sign-function as well as a novel PLL based on the complex band pass filter. There is a common practice in position sensorless control of IPMSMs to use the PLL method together with the EMF, but the PLL method also fails the EMF cannot be accurately estimated at very low or zero speed. In [20], an enhanced SMO including the hyperbolic tangent function with the fuzzy adaptive shape coefficient and estimating rotor speed and position is realized to resolve the chattering and current measurement errors. To improve its ability to predict position and speed more accurately and to increase the rotor's robustness against system uncertainty, it is suggested to use an adaptive filter in an accurate discrete-time SMO in [20]. Moreover, while [21] proposes a frequency-adaptive notch filter utilizing delay signal cancellation to reduce the back EMF harmonics in SMO and the rotor position prediction error, [22] introduces a novel SMO based on a complex-coefficient synchronous frequency filter combined with a quadrature PLL for improving the observation performance till 5% rated speed (75 r/min). However, none of these studies [19–23] based on SMO have been able to provide the prediction results of the rotor position at standstill or very low speed for IPMSMs, since they need an additional signal injection-based position prediction algorithms.

The primary purpose of this study is to introduce an HF voltage injection based SMO and PLL estimator in order to accurately estimate the EEMF, rotor velocity, and rotor position of an IPMSM in a vast range of speeds comprising very low speed and standstill and to perform a reliable and accurate position sensorless speed control of IPMSM with the utilization of the proposed SMO and PLL working under the HF voltage injection. Thus, in the scope of this paper, it is the first time:

- a model-based observer such as SMO and PLL is developed, operated, and tested in real time under the HF voltage injection which does not require an additional signal injection based position estimating algorithm.
- the HF voltage injection method is developed without the use of any other signal processing algorithms, which streamline the design stages and lessen the workload in computing of the sensorless control system.
-the experimental results conducted on an IPMSM of 0.4 kW and 8-pole under no-load and loaded conditions in this paper are unique and superior than those of the real-time based studies using the conventional SMO and PLL in the literature.
- the previous study in [24] is extended with developments of the HF voltage injection based SMO and PLL estimator; stability analysis; real-time implementations and experimental outcomes of the proposed HF voltage injection based SMO and PLL and the position sensorless control system; and performance comparison of the proposed voltage injection-based SMO and PLL and the conventional SMO and PLL for very low and zero speed reversals.

This paper is organized as follows: First of all, Section 1 summarizes the past studies related to position sensorless control literature of IPMSMs. Next, Section 2 explains the dynamic model of the IPMSM, the position sensorless VC system of IPMSM, conventional SMO design, and developments of the proposed voltage injection based SMO and PLL type estimator for estimations of EEMF, rotor speed, and rotor position, respectively. Later, the Experimental setup and results are presented in Section 3. Finally, Section 4 gives the conclusions.

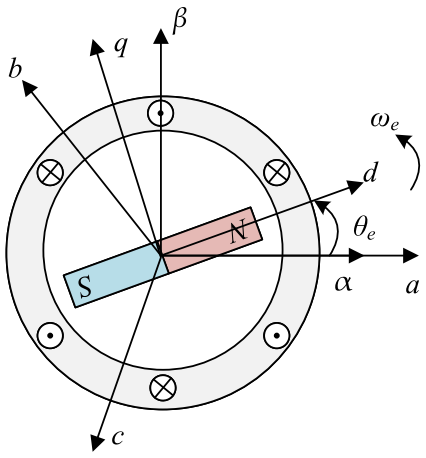

Fig. 1. The reference frame definitions of the IPMSM.

2. Position sensorless control of IPMSM

Position sensorless control method utilizing the dynamic models of IPMSMs is preferable for electric drives due to its cost-effectiveness, mechanical robustness, reduced hardware complexity, and reliability of overall drive system; However, its performance depends on how accurately the speed and/or position is predicted by the proposed sensorless method together with the developed dynamic model of IPMSMs.

2.1. Dynamic model of the IPMSM

A diagram showing a simple magnet and winding orientations for an IPMSM is provided in Fig. 1. Here, the $\alpha\beta$ frame symbolizes the stator stationary reference axis, whereas the dq-frame is rotating at the synchronous speed. Notably, the d-axis aligns with the rotor's flux. θ_e and ω_e are the rotor electrical position and velocity, respectively.

According to Fig. 1, the dynamic model [25] of an IPMSM can be given in the $\alpha\beta$-frame as

$$\begin{bmatrix} u_\alpha \\ u_\beta \end{bmatrix} = R_s \begin{bmatrix} i_\alpha \\ i_\beta \end{bmatrix} + \begin{bmatrix} \Sigma L + \Delta L\cos 2\theta_e & \Delta L \sin 2\theta_e \\ \Delta L \sin 2\theta_e & \Sigma L - \Delta L \cos 2\theta_e \end{bmatrix} p \begin{bmatrix} i_\alpha \\ i_\beta \end{bmatrix} + 2\Delta L \omega_e \begin{bmatrix} -\sin 2\theta_e & \cos 2\theta_e \\ \cos 2\theta_e & \sin 2\theta_e \end{bmatrix} \begin{bmatrix} i_\alpha \\ i_\beta \end{bmatrix} + \omega_e \lambda_{pm} \begin{bmatrix} -\sin\theta_e \\ \cos\theta_e \end{bmatrix} \quad (1)$$

where i_α and i_β and u_α and u_β are the stator currents and stator voltages in the $\alpha\beta$-axis, respectively; R_s is the stator resistance; L_d and L_q are the dq-frame inductances; $\Sigma L = (L_d + L_q)/2$; and $\Delta L = (L_d - L_q)/2$ are the average and differential inductances respectively and p is the differential operator.

In order to directly estimate θ_e, the EEMF based model [26] of IPMSM can be obtained by rewriting Eq. (1) including both $2\theta_e$ and θ_e as below:

$$\begin{bmatrix} u_\alpha \\ u_\beta \end{bmatrix} = \begin{bmatrix} R_s + pL_d & \omega_e(L_d - L_q) \\ -\omega_e(L_d - L_q) & R_s + pL_d \end{bmatrix} \begin{bmatrix} i_\alpha \\ i_\beta \end{bmatrix} + \begin{bmatrix} e_\alpha \\ e_\beta \end{bmatrix} \quad (2)$$

In Eq. (2), the EEMF components (e_α and e_β) consisting of only θ_e are as follows:

$$\begin{bmatrix} e_\alpha \\ e_\beta \end{bmatrix} = \Gamma \begin{bmatrix} -\sin\theta_e \\ \cos\theta_e \end{bmatrix}, \Gamma = (L_d - L_q)(\omega_e i_d - \frac{di_q}{dt}) + \omega_e \lambda_{pm} \quad (3)$$

where λ_{pm} is the PM flux linkage; Γ is the speed dependent EEMF gain; and i_d and i_q are stator currents in the dq-frame, respectively. Please note that the derivative term in the EEMF (Eq. (3)) is effective even at the very low and zero speed ranges; Hence, it is useful for estimating the speed and position with signal injection.

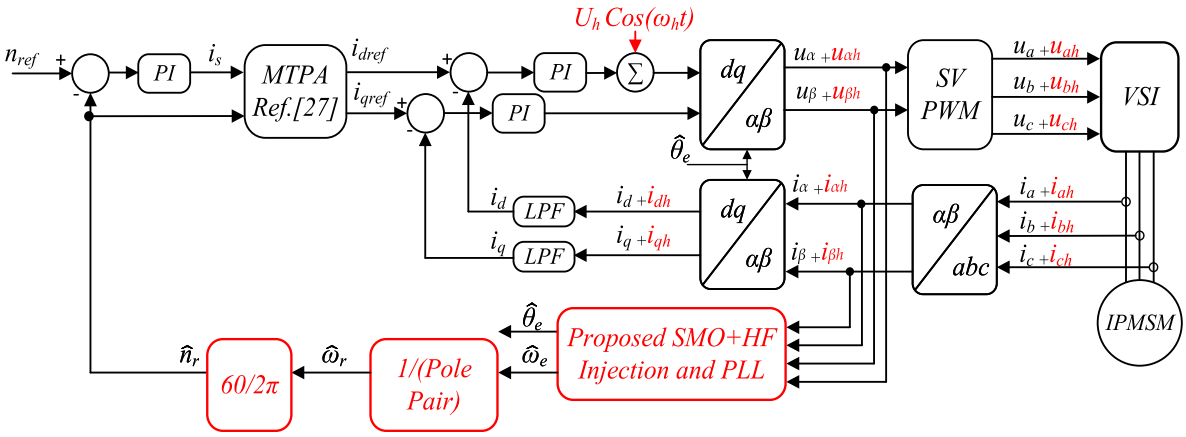

Fig. 2. The sensorless IPMSM vector control block diagram.

Finally, the state model [26] of the IPMSM can be obtained by

$$\begin{aligned} \dot{i}_\alpha &= -\frac{R_s}{L_d} i_\alpha - \frac{\omega_e (L_d - L_q)}{L_d} i_\beta + \frac{u_\alpha}{L_d} - \frac{e_\alpha}{L_d} \\ \dot{i}_\beta &= -\frac{R_s}{L_d} i_\beta + \frac{\omega_e (L_d - L_q)}{L_d} i_\alpha + \frac{u_\beta}{L_d} - \frac{e_\beta}{L_d} \end{aligned} \tag{4}$$

Here, when $L_d = L_q$, Eq. (4) reduces into the equation of surface mounted PMSM (SPMSM) or when $\lambda_{pm} = 0$, Eq. (4) becomes the equation of synchronous reluctance machine (SynRM).

2.2. Position sensorless VC system of the IPMSM

In vector control (VC) of SPMSM, $i_d = 0$ control approach is used for maximum torque per ampere (MTPA) operation [27]. However, the sensorless VC of IPMSM in this paper requires a non-zero i_d for MTPA, as shown in Fig. 2. In Fig. 2,

- the MTPA strategy adjusts the reference values (i_{dref} and i_{qref}) of i_d and i_q in order to enable the attainment of the MTPA operating point of the IPMSM aligning with the torque requirements set by the VC system.
- there are the cascaded inner current regulation loops and the outer speed control loop. The PI-speed controller output is the phase current amplitude ($|i_s|$) which then goes into the MTPA block that calculates i_{dref} and i_{qref}.
- the rotor speed and flux position together with the current sensor signals are required. In this work, an observer that combines SMO and PLL with a high-frequency voltage injection is proposed to provide accurate speed and position estimation in a vast range of speeds including the very low speed and standstill for high-performance control of IPMSMs.

2.3. Conventional SMO design

The conventional SMO structure by utilizing the state model in (4) [26,28] can be given as

$$\begin{aligned} \dot{\hat{i}}_\alpha &= -\frac{R_s}{L_d} \hat{i}_\alpha - \frac{\hat{\omega}_e (L_d - L_q)}{L_d} \hat{i}_\beta + \frac{u_\alpha}{L_d} - \frac{\mu_1 F(\tilde{i}_\alpha)}{L_d} \\ \dot{\hat{i}}_\beta &= -\frac{R_s}{L_d} \hat{i}_\beta + \frac{\hat{\omega}_e (L_d - L_q)}{L_d} \hat{i}_\alpha + \frac{u_\beta}{L_d} - \frac{\mu_2 F(\tilde{i}_\beta)}{L_d} \end{aligned} \tag{5}$$

where ($\hat{i}_\alpha$) and ($\hat{i}_\beta$) are the estimated current value; μ_1 and μ_2 are the observer gains; $F(s_x)$ is the signum function but in order to overcome the chattering, the signum function is changed with the sigmoid function in the SMO, which is defined as

$$F(s_x) = \frac{1 - e^{-\sigma s_x}}{1 + e^{-\sigma s_x}} \tag{6}$$

where σ is a positive parameter; and s_x represents the sliding surface selected on the stator current's prediction error and is defined as

$$\begin{aligned} s_\alpha &= \tilde{i}_\alpha = \hat{i}_\alpha - i_\alpha \\ s_\beta &= \tilde{i}_\beta = \hat{i}_\beta - i_\beta \end{aligned} \tag{7}$$

The estimation error dynamics can be written by taking the difference between Eqs. (5) and (4).

$$\begin{aligned} \dot{\tilde{i}}_\alpha &= -\frac{R_s}{L_d} \tilde{i}_\alpha - \frac{(L_d - L_q)}{L_d} (\hat{\omega}_e \hat{i}_\beta - \omega_e i_\beta) + \frac{e_\alpha - \mu_1 F(\tilde{i}_\alpha)}{L_d} \\ \dot{\tilde{i}}_\beta &= -\frac{R_s}{L_d} \tilde{i}_\beta + \frac{(L_d - L_q)}{L_d} (\hat{\omega}_e \hat{i}_\alpha - \omega_e i_\alpha) + \frac{e_\beta - \mu_1 F(\tilde{i}_\beta)}{L_d} \end{aligned} \tag{8}$$

For analyzing the stability of the error dynamics in (8), a Lyapunov function is defined by

$$V_1 = \frac{s_{\alpha\beta}^T s_{\alpha\beta}}{2} = \frac{\tilde{i}_\alpha^2 + \tilde{i}_\beta^2}{2} \tag{9}$$

where $s_{\alpha\beta} = \begin{bmatrix} s_\alpha \\ s_\beta \end{bmatrix}$. The stability condition for the SMO can be obtained from the time-derivative of (9) as

$$\dot{V}_1 = \tilde{i}_\alpha \dot{\tilde{i}}_\alpha + \tilde{i}_\beta \dot{\tilde{i}}_\beta \le 0 \tag{10}$$

Substituting (8) into (10) and taking $\sigma \gg 1$, (10) is rewritten as below [26,28]:

$$\dot{V}_1 = -\frac{R_s}{L_d} (\tilde{i}_\alpha^2 + \tilde{i}_\beta^2) + \frac{\tilde{i}_\alpha}{Ld} (e_\alpha - \mu_1 F(\tilde{i}_\alpha)) + \frac{\tilde{i}_\beta}{Ld} (e_\beta - \mu_2 F(\tilde{i}_\beta)) \le 0 \tag{11}$$

For verification of the stability of the conventional SMO, the observer gains μ_1 and μ_2 should be selected large enough to satisfy (12):

$$\mu_1 F(\tilde{i}_\alpha) > max(|e_\alpha|), \mu_2 F(\tilde{i}_\beta) > max(|e_\beta|) \tag{12}$$

When (12) is satisfied by selecting appropriate μ_1 and μ_2, the system will reach the sliding surface ($s_\alpha = 0$ and $s_\beta = 0$) and then the following criteria are derived by using (4) and (5):

$$\hat{e}_\alpha = \mu_1 F(s_\alpha), \hat{e}_\beta = \mu_2 F(s_\beta) \tag{13}$$

2.4. The proposed voltage injection based SMO and PLL for EEMF, speed, and position estimation

Conventionally, the SMO estimating the EEMF terms and then PLL uses these estimated EEMF terms to perform the simultaneous estimations of rotor velocity and position; Thus, the conventional SMO with PLL needs reasonably accurate stator voltages u_α and u_β for a desirable estimation performance. However, at very low speeds, u_α and u_β are extremely small, making the strong effect of inverter nonlinearities on

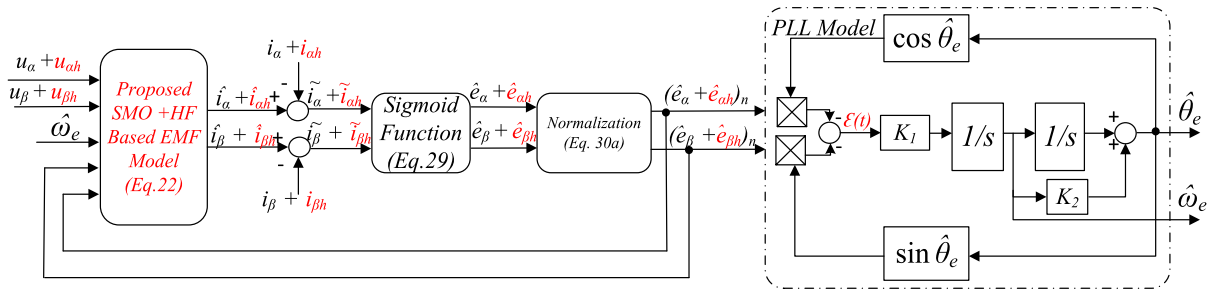

Fig. 3. Sliding mode observer with PLL structure.

system behavior inevitable, which can lead to instability in both the observer and the drive system. To address this issue, the HF injection method is employed to improve the estimation of EEMF as well as position estimation. In this paper, for the first time, an HF voltage injection-based SMO is developed and combined with a PLL for the online estimation of rotor speed and position. In the proposed SMO, the high-frequency voltage is inserted only on d- axis in order to prevent torque ripple due to the HF current in q-axis; The purpose of the voltage injection is to strengthen the attenuated EEMF signal by providing phase alignment at standstill and low speed and to improve the very low/zero speed estimation performance of the conventional SMO with PLL. For this aim, firstly the cosinusoidal HF voltage in (14) is inserted into dq-frame, as shown in Fig. 2:

$$\begin{bmatrix} u_{dh} \\ u_{qh} \end{bmatrix} = \begin{bmatrix} U_h \cos \omega_h t \\ 0 \end{bmatrix} \tag{14}$$

where u_{dh} and u_{qh} are the injected signals to the reference voltages; U_h and ω_h are the magnitude and the inserted voltage's frequency, respectively.

Next, (14) are transformed into the $\alpha\beta$-frame as

$$\begin{bmatrix} u_{\alpha h} \\ u_{\beta h} \end{bmatrix} = \begin{bmatrix} u_{dh} \cos \theta_e \\ u_{qh} \sin \theta_e \end{bmatrix} \tag{15}$$

Then, differently from [29] using dq-model of IPMSM, signal processing algorithms, and not depending on EEMF, this paper proposes to utilize the $\alpha\beta$ model with the EEMF term of IPMSM in (2). As seen in Fig. 2, since (15) is added to the main driving voltages (u_α and u_β), the $\alpha\beta$ model in (2) becomes as below:

$$\begin{bmatrix} u_\alpha + u_{\alpha h} \\ u_\beta + u_{\beta h} \end{bmatrix} = \begin{bmatrix} R_s + pL_d & \omega_e(L_d - L_q) \\ -\omega_e(L_d - L_q) & R_s + pL_d \end{bmatrix} \times \begin{bmatrix} i_\alpha + i_{\alpha h} \\ i_\beta + i_{\beta h} \end{bmatrix} + \begin{bmatrix} e_\alpha + e_{\alpha h} \\ e_\beta + e_{\beta h} \end{bmatrix} \tag{16}$$

where $i_{\alpha h}, i_{\beta h}, u_{\alpha h}, u_{\beta h}, e_{\alpha h}, e_{\beta h}$ are the HF terms of currents, voltages, and the EEMF values in the $\alpha\beta$ axis, respectively. Later, the counterpart of (3), which is the components of EEMF with the HF terms in (16), can be derived by considering (1) with the HF terms as below:

$$\begin{aligned} \begin{bmatrix} e_\alpha + e_{\alpha h} \\ e_\beta + e_{\beta h} \end{bmatrix} &= 2\Delta L \begin{bmatrix} -\sin^2\theta_e & \sin\theta_e \cos\theta_e \\ \sin\theta_e \cos\theta_e & -\cos^2\theta_e \end{bmatrix} p \begin{bmatrix} i_\alpha + i_{\alpha h} \\ i_\beta + i_{\beta h} \end{bmatrix} \\ &+ 4\omega_e \Delta L \begin{bmatrix} -\sin\theta_e \cos\theta_e & -\sin^2\theta_e \\ \cos^2\theta_e & \sin\theta_e \cos\theta_e \end{bmatrix} \begin{bmatrix} i_\alpha + i_{\alpha h} \\ i_\beta + i_{\beta h} \end{bmatrix} \\ &+ \omega_e \lambda_{pm} \begin{bmatrix} -\sin\theta_e \\ \cos\theta_e \end{bmatrix} \end{aligned} \tag{17}$$

Thus, considering the injected voltage vector in the $\alpha\beta$ frame separately and neglecting the ω_e-dependent terms in (17) since the HF voltage injection will be used at the very low and zero speeds, the HF voltage part of (16) becomes

$$\begin{bmatrix} u_{\alpha h} \\ u_{\beta h} \end{bmatrix} = \begin{bmatrix} R_s + pL_d & 0 \\ 0 & R_s + pL_d \end{bmatrix} \begin{bmatrix} i_{\alpha h} \\ i_{\beta h} \end{bmatrix} + \begin{bmatrix} e_{\alpha h} \\ e_{\beta h} \end{bmatrix} \tag{18}$$

where,

$$\begin{aligned} \begin{bmatrix} e_{\alpha h} \\ e_{\beta h} \end{bmatrix} &= 2\Delta L \begin{bmatrix} -\sin^2\theta_e & \sin\theta_e \cos\theta_e \\ \sin\theta_e \cos\theta_e & -\cos^2\theta_e \end{bmatrix} p \begin{bmatrix} i_{\alpha h} \\ i_{\beta h} \end{bmatrix} \\ &\approx -2\Delta L \frac{di_{qh}}{dt} \begin{bmatrix} -\sin\theta_e \\ \cos\theta_e \end{bmatrix} = (\Gamma_h) \begin{bmatrix} -\sin\theta_e \\ \cos\theta_e \end{bmatrix} \end{aligned} \tag{19}$$

The main driving voltage part (without the HF terms) of (16) is exactly as in (2) and (3). Finally, the EEMF components in (17) including the effects of both HF voltage injection and main driving voltage can be written as

$$\begin{bmatrix} e_\alpha + e_{\alpha h} \\ e_\beta + e_{\beta h} \end{bmatrix} = (\Gamma + \Gamma_h) \begin{bmatrix} -\sin\theta_e \\ \cos\theta_e \end{bmatrix} \tag{20}$$

where, Γ_h is defined as in (19) and represents the HF term of EEMF because of the injected HF voltage.

Now, it is time to design a suitable SMO estimator in order to estimate the EEMF components in (20) and a PLL for the estimations of the rotor velocity and position. For this aim, (16) can be given in state space form as in (21):

$$\begin{aligned} \dot{i}_\alpha + \dot{i}_{\alpha h} &= -\frac{R_s}{L_d}(i_\alpha + i_{\alpha h}) - \frac{\omega_e(L_d - L_q)}{L_d}(i_\beta + i_{\beta h}) + \frac{u_\alpha + u_{\alpha h}}{L_d} - \frac{e_\alpha + e_{\alpha h}}{L_d} \\ \dot{i}_\beta + \dot{i}_{\beta h} &= -\frac{R_s}{L_d}(i_\beta + i_{\beta h}) + \frac{\omega_e(L_d - L_q)}{L_d}(i_\alpha + i_{\alpha h}) + \frac{u_\beta + u_{\beta h}}{L_d} - \frac{e_\beta + e_{\beta h}}{L_d} \end{aligned} \tag{21}$$

The proposed SMO structure by using the state model in (21) can be given as

$$\begin{aligned} \dot{\hat{i}}_\alpha + \dot{\hat{i}}_{\alpha h} &= -\frac{R_s}{L_d}(\hat{i}_\alpha + \hat{i}_{\alpha h}) - \frac{\omega_e(L_d - L_q)}{L_d}(i_\beta + i_{\beta h}) + \frac{u_\alpha + u_{\alpha h}}{L_d} - \frac{\mu_1 F(\tilde{i}_\alpha + \tilde{i}_{\alpha_h})}{L_d} \\ \dot{\hat{i}}_\beta + \dot{\hat{i}}_{\beta h} &= -\frac{R_s}{L_d}(\hat{i}_\beta + \hat{i}_{\beta h}) - \frac{\omega_e(L_d - L_q)}{L_d}(i_\alpha + i_{\alpha h}) + \frac{u_\beta + u_{\beta h}}{L_d} - \frac{\mu_2 F(\tilde{i}_\beta + \tilde{i}_{\beta h})}{L_d} \end{aligned} \tag{22}$$

Again, considering the HF part of (22) separately and neglecting the ω_e-dependent terms, (22) becomes

$$\begin{aligned} \dot{\hat{i}}_{\alpha h} &= -\frac{R_s}{L_d}\hat{i}_{\alpha h} + \frac{u_{\alpha h}}{L_d} - \frac{\mu_1 F(\tilde{i}_{\alpha h})}{L_d} \\ \dot{\hat{i}}_{\beta h} &= -\frac{R_s}{L_d}\hat{i}_{\beta h} + \frac{u_{\beta h}}{L_d} - \frac{\mu_2 F(\tilde{i}_{\beta h})}{L_d} \end{aligned} \tag{23}$$

Then, the error dynamics can be expressed as:

$$\begin{aligned} \dot{\tilde{i}}_{\alpha h} &= -\frac{R_s}{L_d}\tilde{i}_{\alpha h} + \frac{e_{\alpha h}}{L_d} - \frac{\mu_1 F(\tilde{i}_{\alpha h})}{L_d} \\ \dot{\tilde{i}}_{\beta h} &= -\frac{R_s}{L_d}\tilde{i}_{\beta h} + \frac{e_{\beta h}}{L_d} - \frac{\mu_2 F(\tilde{i}_{\beta h})}{L_d} \end{aligned} \tag{24}$$

For analyzing the stability of the error dynamics in (24), a Lyapunov function is defined by

$$V_2 = \frac{s_{\alpha\beta h}^T s_{\alpha\beta h}}{2} = \frac{\tilde{i}_{\alpha h}^2 + \tilde{i}_{\beta h}^2}{2} \tag{25}$$

where $s_{\alpha\beta h} = \begin{bmatrix} s_{\alpha h} \\ s_{\beta h} \end{bmatrix}$. The stability condition for the SMO can be obtained from the time-derivative of (25) as

$$\dot{V}_2 = \tilde{i}_{\alpha h}\dot{\tilde{i}}_{\alpha h} + \tilde{i}_{\beta h}\dot{\tilde{i}}_{\beta h} \le 0 \tag{26}$$

(24) is substituted into (26), and (26) becomes

$$\begin{aligned} \dot{V}_2 = -\frac{R_s}{L_d}(\tilde{i}_{\alpha h}^2 + \tilde{i}_{\beta h}^2) + \frac{\tilde{i}_{\alpha h}}{Ld}(e_{\alpha h} - \mu_1 F(\tilde{i}_{\alpha h})) \\ + \frac{\tilde{i}_{\beta h}}{Ld}(e_{\beta h} - \mu_2 F(\tilde{i}_{\beta h})) \le 0 \end{aligned} \tag{27}$$

To determine the stability of the proposed SMO, the observer gains μ_1 and μ_2 should be selected large enough to satisfy following both conditions at the same time:

$$\begin{aligned} &\mu_1 F(\tilde{i}_{\alpha h}) > max(|e_{\alpha h}|), \mu_2 F(\tilde{i}_{\beta h}) > max(|e_{\beta h}|) \\ &\qquad \text{for the HF part} \\ &\mu_1 F(\tilde{i}_{\alpha}) > max(|e_{\alpha}|), \mu_2 F(\tilde{i}_{\beta}) > max(|e_{\beta}|) \\ &\qquad \text{for the main part} \end{aligned} \tag{28}$$

When (28) is satisfied by selecting appropriate μ_1 and μ_2, the system will reach the sliding surface and then the following criteria providing the estimated EEMF terms are valid by using (21) and (22):

$$\begin{aligned} \hat{e}_{\alpha} + \hat{e}_{\alpha h} &= \mu_1 F(\tilde{i}_{\alpha} + \tilde{i}_{\alpha h}) \\ \hat{e}_{\beta} + \hat{e}_{\beta h} &= \mu_2 F(\tilde{i}_{\beta} + \tilde{i}_{\beta h}) \end{aligned} \tag{29}$$

Here, F is the sigmoid function as defined in (6).

Finally, the estimations of ω_e and θ_e are performed by substituting $\hat{e}_{\alpha} + \hat{e}_{\alpha h}$ and $\hat{e}_{\beta} + \hat{e}_{\beta h}$ in (29), which can be also considered as (20), into the angle tracking (PLL) algorithm as shown in Fig. 3, where $(\hat{\theta}_e, \hat{\omega}_e)$ are estimations of (θ_e, ω_e), respectively; K_1 and K_2 are positive constant gains; $\hat{\omega}_e = \frac{d\theta_e}{dt}$, and $\epsilon(t)$ denotes estimation error for the rotor electrical position and is defined as

$$\begin{aligned} (\hat{e}_{\alpha} + \hat{e}_{\alpha h})_n &= \frac{1}{\sqrt{(\hat{e}_{\alpha} + \hat{e}_{\alpha h})^2 + (\hat{e}_{\beta} + \hat{e}_{\beta h})^2}}(\hat{e}_{\alpha} + \hat{e}_{\alpha h}) \\ (\hat{e}_{\beta} + \hat{e}_{\beta h})_n &= \frac{1}{\sqrt{(\hat{e}_{\alpha} + \hat{e}_{\alpha h})^2 + (\hat{e}_{\beta} + \hat{e}_{\beta h})^2}}(\hat{e}_{\beta} + \hat{e}_{\beta h}) \end{aligned} \tag{30a}$$

$$\epsilon(t) = -[(\hat{e}_{\alpha} + \hat{e}_{\alpha h})_n \cos\hat{\theta}_e + (\hat{e}_{\beta} + \hat{e}_{\beta h})_n \sin\hat{\theta}_e] \tag{30b}$$

The estimated EEMF in (29) can be also given in terms of (20) as below:

$$\begin{aligned} \hat{e}_{\alpha} + \hat{e}_{\alpha h} &= -(\Gamma + \Gamma_h)\sin\theta_e \\ \hat{e}_{\beta} + \hat{e}_{\beta h} &= (\Gamma + \Gamma_h)\cos\theta_e \end{aligned} \tag{31}$$

Substituting (31) into (30) results in

$$\begin{aligned} \epsilon(t) &= (\sin\theta_e \cos\hat{\theta}_e - \cos\theta_e \sin\hat{\theta}_e) \\ &= \sin(\theta_e - \hat{\theta}_e) \approx \theta_e - \hat{\theta}_e \end{aligned} \tag{32}$$

When $\epsilon(t)$ goes to zero with the help of the implementation including the integrator and the PI controller, which are connected in series and enclosed within a unit feedback loop as seen in Fig. 3, $\hat{\theta}_e$ converges to θ_e.

Now, the closed-loop PLL transfer function can be given as below:

$$\frac{\hat{\theta}_e}{\theta_e} = \frac{(K_1 + K_1 K_2 s)}{s^2 + K_1 K_2 s + K_1} \tag{33}$$

Table 1
IPMSM parameters.

Parameters	Values
R_s	23.5 Ω
L_d	56 mH
L_q	125 mH
λ_{pm}	0.165 Wb
Rated speed	3000 rpm
Rated load	1.4 N m
P	8
J	0.03 kg m^2

where, K_1 and K_2 are the coefficients that affect the dynamic performance of the PLL estimator. For a stable operation with an acceptable estimation error, these coefficients should be selected according to the typical second order system as

$$G(s) = \frac{\omega_n^2}{s^2 + 2\zeta\omega_n s + \omega_n^2} \tag{34}$$

where ζ is the damping factor and ω_n is the natural frequency. After determining the desired response characteristics for the general second order system, the PLL coefficients K_1 and K_2 can be computed as $K_1 = \omega_n^2$ and $K_2 = 2\zeta/\omega_n$.

Thus, the complete diagram of the proposed voltage signal injection based SMO and PLL to effectively estimate the EEMF, rotor speed and rotor position is given in Fig. 3 for a reliable and accurate position sensorless control of IPMSM.

3. The experimental setup and results

A comprehensive evaluation of the position sensorless IPMSM drive using both proposed HF voltage signal injection based SMO&PLL and conventional SMO are implemented in real time as shown in Figs. 4 and 5, respectively, for exhibiting the tracking performance of the proposed SMO and PLL compared to the conventional SMO and PLL. In the experimental setup,

- the parameters of the utilized IPMSM are given in Table 1.
- the proposed or conventional estimation method along with the vector control algorithm is embedded in a Texas Instruments of TMS320F28379D DSP that can process floating and fixed-point operations at a rate of 200 MHz.
- Texas Instruments TMDXIDDK379D Design Drive development kit is used as the inverter.
- the inverter's switching frequency is f_s = 10 kHz and the control period is 100 μs.
- a torque transducer of 20 N m is interposed between the IPMSM and the dynamometer for load torque measurements.
- the actual speed and rotor position are measured with a resolver integrated into the motor for validating the estimated rotor position and velocity.
- the actual and predicted values of the speed and position are sent to the oscilloscope with digital analog converter outputs of the DSP for observing and data collecting.

For the initialization of the proposed and conventional estimation algorithms,

- it is observed that the inserted HF voltage's frequency lessens the effect on the accurateness of the estimations because of the reduced stator currents while the boosted amplitude of the injected HF voltage causes the increased fluctuations in the stator current, which results in the amplified noise of the operation. Consequently, the magnitude and the angular frequency of the inserted voltage are selected as U_h = 25 V and $\omega_h = 1000\pi$ rad/s, respectively, considering these effects.
- the SMO parameters are selected so that the estimation output is accurate and experiences as low chattering noise as possible; Thus, the observer gains are determined as $\mu_1 = \mu_2$ = 31 500 and the sigmoid coefficient is taken as σ = 0.001.

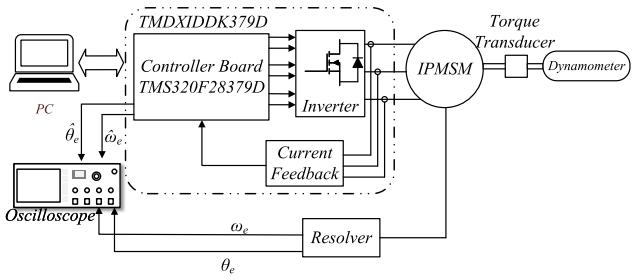

Fig. 4. The experimental setup's schematic representation.

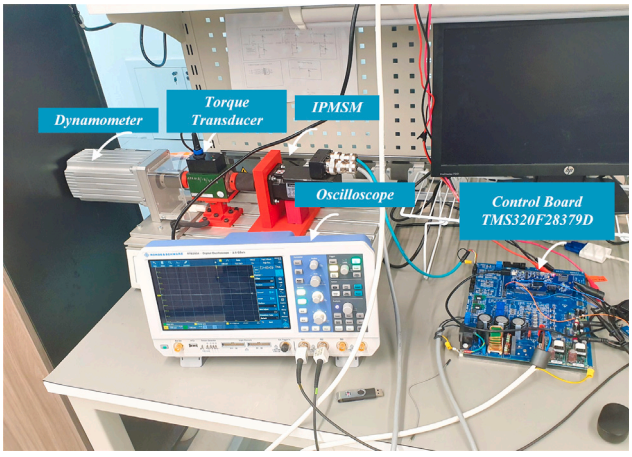

Fig. 5. The view of the experimental setup.

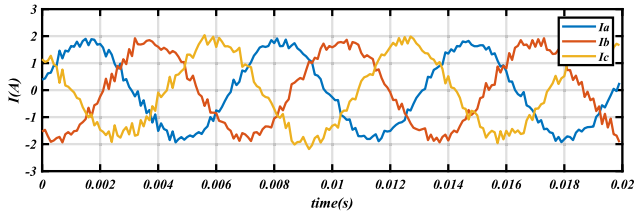

Fig. 6. The HF current response under loaded condition.

- the PLL gains are calculated using (27) for a non-overshoot response and around 200 Hz bandwidth, and then $\zeta = 1$ and $\omega_n = 500$ are determined; Therefore, the PLL coefficients are calculated as $K_1 = 250\,000$ and $K_2 = 0.0016$.
- the bus voltage is applied as $V_{DC} = 250$ V in order to operate the experimental setup.

The current response when the proposed HF voltage injection based SMO & PLL is applied is shown in Fig. 6.

The efficacy of the proposed voltage injection-based SMO and PLL are tested by using different challenging scenarios in a wide speed range including standstill and very low speed as follows:

Scenario 1 (Fig. 7): Performances for high speed reversal under step-like variations in the load torque.

In this scenario, the estimation performance of the proposed voltage injection-based SMO and PLL is checked under the step-like variable load torque in a wide speed range including zero crossover in both clockwise (CW) and counter clockwise (CCW) rotations, as illustrated in Fig. 7 where the HF voltage of 25 cos(1000πt) is injected on d- axis at 150 rpm in order to enhance the prediction performance at very low speeds and zero crossover. Inspecting the estimation error given in Fig. 7(c), it is clear that the estimated speed closely tracks the actual

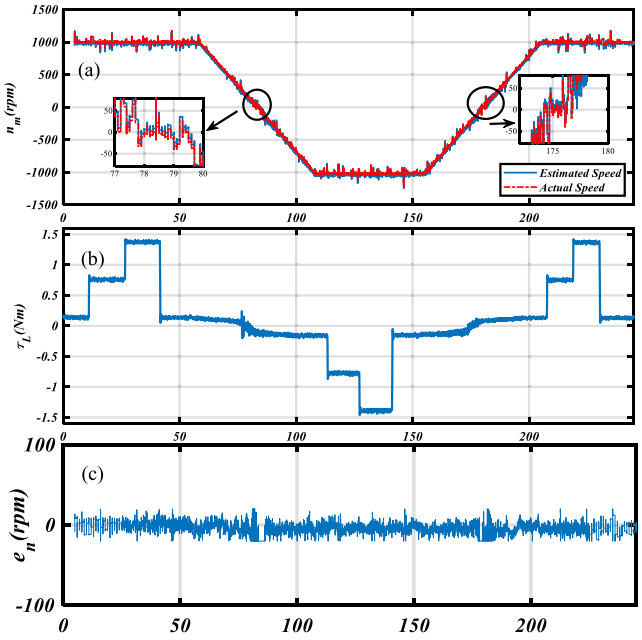

Fig. 7. Real-time speed estimation performance of the proposed voltage injection-based SMO and PLL for Scenario 1. (a) variations of the actual and estimated speeds (b) variation of the load torque, and (c) variation of the speed estimation error.

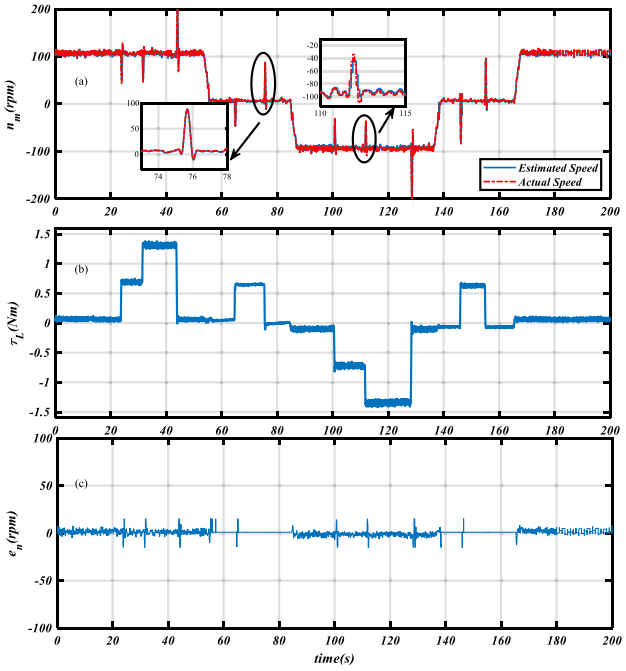

Fig. 8. Real-time speed prediction performance of the proposed voltage injection-based SMO and PLL for Scenario 2. (a) variations of the actual and estimated speeds (b) variation of the load torque, and (c) variation of the speed estimation error.

motor speed in all operating ranges of the IPMSMs for this scenario even when the speed approaches and crosses zero.

Scenario 2 (Fig. 8): Performances for very low and zero speed reversal under step-like variations in the load torque

This scenario aims to test the estimation performance of the proposed voltage injection-based SMO and PLL under the instant load torque variations at standstill and low speed which is the most challenging scenario for the observers using the fundamental model of IPMSM in the literature. Therefore, the IPMSM is operated by injecting

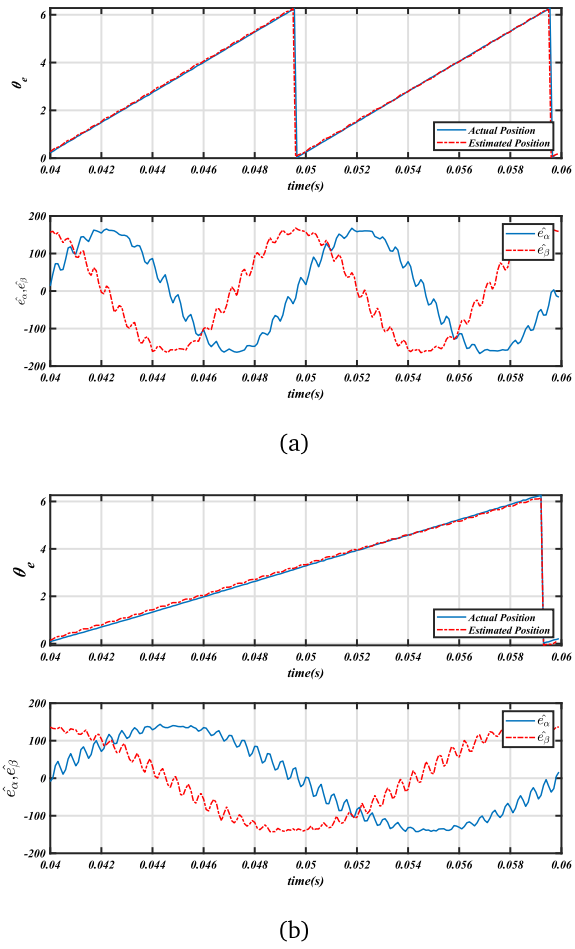

(a)

(b)

Fig. 9. EMF and position estimation performance of the proposed voltage injection-based SMO and PLL for Scenario 3. (a) 300 rpm speed, and (b) 150 rpm speed.

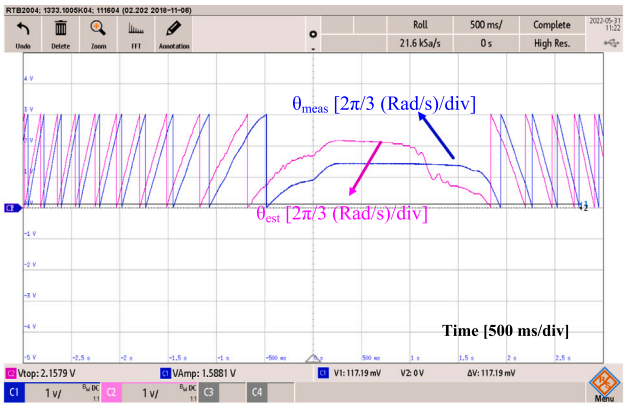

(a)

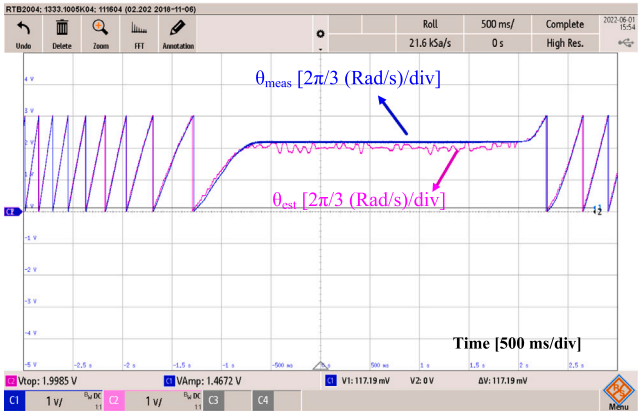

(b)

Fig. 10. The real-time comparison results of the rotor position estimations during low and zero speed region for Scenario 3. (a) the conventional SMO and PLL (without voltage signal injection) working in the open loop, (b) the proposed HF voltage injection based SMO and PLL operated in the closed loop VC system as in Fig. 2.

the HF voltage of 25 $\cos(1000\pi t)$ on d- axis at zero and 100 rpm in the directions of both CW and CCW under no-load and the instant load torque variations, as demonstrated in Fig. 8. In spite of the most difficult scenario, the proposed HF voltage injection based SMO and PLL is able to satisfactorily estimate the actual rotor speed, as seen in Fig. 7(c). It should be also noted that real-time experimental results in Fig. 7, which are the first in the current literature related to the position sensorless AC drive using only the fundamental model of IPMSMs, are obtained due to the voltage injection based SMO proposed by this paper.

Scenario 3 (Fig. 9): Performances in low speed region for Estimated position and EMF under loaded condition

This scenario aims to show the estimation performance of the proposed voltage injection-based SMO and PLL at low speeds illustrating the impact of the proposed method on the estimation of electromotive force (EMF) and position. It is important to note that direct measurement of actual back EMF values in $\alpha\beta$ frame is impractical, due to their dependence on rotor speed and flux linkage. For this purpose, the IPMSM is operated by inserting the HF voltage on d- axis at 300 rpm and 150 rpm in the CW direction under loaded condition, as depicted in Fig. 9. The obtained results indicate that the proposed voltage injection-based SMO and PLL presented in this paper is capable of accurately tracking the actual position, with acceptable estimation performance.

Scenario 4 (Fig. 10): Performance Comparison of the proposed voltage injection-based SMO and PLL and the conventional SMO and PLL for very low and zero speed reversals.

This scenario aims to compare through the estimated rotor positions obtained by both proposed HF voltage injection based SMO&PLL and conventional SMO and PLL specifically at very low and zero speed in the CW and CCW directions in order to reveal the superiority of the proposed method over the conventional one. Thus,

- while the IPMSM firstly runs with the utilization of the actual rotor position under the VC system, the conventional SMO and PLL described in paragraph 2.3 is operated by utilizing the measured stator currents and voltages of the VC system in the open loop where the estimated rotor position of the conventional SMO and PLL is not used as feedback to the VC system and is only monitored for a comparison purpose since the conventional method is not able to be operated at standstill and very low speeds.
-later, the IPMSM is operated by using the proposed HF voltage injection based SMO and PLL in the closed loop as shown in Fig. 2.

Finally, the real-time experimental results related to the estimated and the actual rotor position of both conventional and proposed methods in this paper are obtained for the cases the rotor speed approaches zero in the CW direction, stays at zero speed for a duration of time, and accelerates in the CCW direction, as given in Fig. 10. Examining the obtained results in Figs. 10(a) and 10(b), the following observations can be made:

- The rotor position estimation error of the conventional SMO and PLL increases and results in the loss of the phase alignment as the rotor speed approaches zero; Thus, it cannot be utilized as feedback

in the closed loop VC system, which is expected and common result as reported by the literature.
- It is clear that the proposed HF voltage injection based SMO and PLL is able to precisely estimate the actual rotor position at very low and zero speeds due to the injected HF voltage on the d- axis amplifying the attenuated EEMF signal, which is the first according to the literature utilizing the fundamental model of IPMSMs. In conclusion, the obtained comparison results verify the superior performance of the proposed HF voltage injection based SMO and PLL over the conventional SMO and PLL.

4. Conclusion

In this paper, it is the first time an SMO based on voltage signal injection and PLL type estimator are presented to the literature for the solution of the rotor position estimation problem associated with the observers using the fundamental model of IPMSM owing to the attenuated and deteriorated EEMF with noise at very low and zero speed. The HF voltage injection method in this paper is established without the use of any other signal processing algorithms, thus it simplifies the design stages and reduces the computational load of the position sensorless VC system. The obtained results from the real-time experimental setup consisting of an 8-pole and 0.4 kW IPMSM under no-load and step-like load torque variations verify that
- the designed closed loop VC system with the utilization of the proposed voltage signal injection-based SMO and PLL is capable to be operated at high, very low and zero speeds.
- the proposed SMO based on voltage signal injection and PLL introduced by this paper has superiority over the conventional SMO and PLL in the literature.

Our next study is going to focus on how to improve dynamic performance of the position sensorless VC system of the IPMSMs.

CRediT authorship contribution statement

Ertugrul Ates: Writing – review & editing, Writing – original draft, Visualization, Validation, Investigation, Formal analysis, Conceptualization. **Burak Tekgun:** Writing – review & editing, Writing – original draft, Supervision, Project administration, Investigation, Conceptualization. **Gunyaz Ablay:** Writing – review & editing, Writing – original draft, Supervision, Conceptualization. **Murat Barut:** Writing – review & editing, Supervision, Conceptualization.

Declaration of competing interest

The authors declare that they have no known competing financial interests or personal relationships that could have appeared to influence the work reported in this paper.

Acknowledgments

The authors wish to acknowledge the support of the scientific and technological research council of Türkiye (TUBITAK) under 2214-A project entitled “Sensorless Control of Interior Permanent Magnet Synchronous Machines”.

References

[1] S. Li, X. Zhou, Sensorless energy conservation control for permanent magnet synchronous motors based on a novel hybrid observer applied in coal conveyer systems, Energies 11 (10) (2018) 1–23, http://dx.doi.org/10.3390/en11102554.
[2] R. Ni, D. Xu, G. Wang, X. Gui, G. Zhang, H. Zhan, C. Li, Efficiency enhancement of general AC drive system by remanufacturing induction motor with interior permanent-magnet rotor, IEEE Trans. Ind. Electron. 63 (2) (2016) 808–820, http://dx.doi.org/10.1109/TIE.2015.2477478.
[3] C.J.V. Filho, D. Xiao, R.P. Vieira, A. Emadi, Observers for high-speed sensorless PMSM drives: Design methods, tuning challenges and future trends, IEEE Access 9 (2021) 56397–56415, http://dx.doi.org/10.1109/ACCESS.2021.3072360.
[4] Y. Zuo, C. Lai, K.L.V. Iyer, A review of sliding mode observer based sensorless control methods for PMSM drive, IEEE Trans. Power Electron. 38 (9) (2023) 11352–11367, http://dx.doi.org/10.1109/TPEL.2023.3287828.
[5] T.F. Chan, P. Borsje, W. Wang, Application of unscented kalman filter to sensorless permanent-magnet synchronous motor drive, in: 2009 IEEE International Electric Machines and Drives Conference, IEMDC ’09, IEEE, 2009, pp. 631–638, http://dx.doi.org/10.1109/IEMDC.2009.5075272.
[6] G. Zhang, G. Wang, B. Yuan, R. Liu, D. Xu, Active disturbance rejection control strategy for signal injection-based sensorless IPMSM drives, IEEE Trans. Transp. Electrif. 4 (1) (2017) 330–339, http://dx.doi.org/10.1109/TTE.2017.2765206.
[7] G. Wang, M. Valla, J. Solsona, Position sensorless permanent magnet synchronous machine drives - A review, IEEE Trans. Ind. Electron. 67 (7) (2020) 5830–5842, http://dx.doi.org/10.1109/TIE.2019.2955409.
[8] P. Vaclavek, P. Blaha, I. Herman, AC drive observability analysis, IEEE Trans. Ind. Electron. 60 (8) (2013) 3047–3059, http://dx.doi.org/10.1109/TIE.2012.2203775.
[9] I. Boldea, M.C. Paicu, G.D. Andreescu, F. Blaabjerg, “Active flux” DTFC-SVM sensorless control of IPMSM, IEEE Trans. Energy Convers. 24 (2) (2009) 314–322, http://dx.doi.org/10.1109/TEC.2009.2016137.
[10] X. Sun, Y. Zhang, X. Tian, J. Cao, J. Zhu, Speed sensorless control for IPMSMs using a modified MRAS with gray wolf optimization algorithm, IEEE Trans. Transp. Electrif. 8 (1) (2022) 1326–1337, http://dx.doi.org/10.1109/TTE.2021.3093580.
[11] M.S. Rafaq, A.T. Nguyen, H.H. Choi, J.W. Jung, A robust high-order disturbance observer design for SDRE-based suboptimal speed controller of interior PMSM drives, IEEE Access 7 (2019) 165671–165683, http://dx.doi.org/10.1109/ACCESS.2019.2953073.
[12] H.S. Kim, S.K. Sul, H. Yoo, J. Oh, Distortion-minimizing flux observer for IPMSM based on frequency-adaptive observers, IEEE Trans. Power Electron. 35 (2) (2020) 2077–2087, http://dx.doi.org/10.1109/TPEL.2019.2920691.
[13] S.M. Gadoue, D. Giaouris, J.W. Finch, MRAS sensorless vector control of an induction motor using new sliding-mode and fuzzy-logic adaptation mechanisms, IEEE Trans. Energy Convers. 25 (2) (2010) 394–402, http://dx.doi.org/10.1109/TEC.2009.2036445.
[14] F. Genduso, R. Miceli, C. Rando, G.R. Galluzzo, Back EMF sensorless-control algorithm for high-dynamic performance PMSM, IEEE Trans. Ind. Electron. 57 (6) (2010) 2092–2100, http://dx.doi.org/10.1109/TIE.2009.2034182.
[15] Z. Chen, M. Tomita, S. Doki, S. Okuma, An extended electromotive force model for sensorless control of interior permanent-magnet synchronous motors, IEEE Trans. Ind. Electron. 50 (2) (2003) 288–295, http://dx.doi.org/10.1109/TIE.2003.809391.
[16] O.C. Kivanc, S.B. Ozturk, Sensorless PMSM drive based on stator feedforward voltage estimation improved with MRAS multiparameter estimation, IEEE/ASME Trans. Mechatronics 23 (3) (2018) 1326–1337, http://dx.doi.org/10.1109/TMECH.2018.2817246.
[17] G. Zhou, L. Sun, L. Qian, Q. Zou, Sensorless predictive control with fusion position estimation technology for PMSM drives, IEEE Trans. Transp. Electrif. PP (2023) 1, http://dx.doi.org/10.1109/TTE.2023.3321369.
[18] J. Hong, S. Jung, K. Nam, An incorporation method of sensorless algorithms: Signal injection and back EMF based methods, in: 2010 International Power Electronics Conference - ECCE Asia -, IPEC 2010, IEEE, 2010, pp. 2743–2747, http://dx.doi.org/10.1109/IPEC.2010.5543188.
[19] Z. Yin, Y. Zhang, X. Cao, D. Yuan, J. Liu, Estimated position error suppression using novel PLL for IPMSM sensorless drives based on full-order SMO, IEEE Trans. Power Electron. 37 (4) (2022) 4463–4474, http://dx.doi.org/10.1109/TPEL.2021.3125024.
[20] S. Ye, X. Yao, An enhanced SMO-based permanent-magnet synchronous machine (PMSM) sensorless drive scheme with current measurement error compensation, IEEE J. Emerg. Sel. Top. Power Electron. 6777 (c) (2020) http://dx.doi.org/10.1109/JESTPE.2020.3038859.
[21] Z. Wu, C. Cheng, W. Hua, Y. Wang, H. Zhang, W. Wang, A frequency-adaptive delay signal cancelation based filter to reduce position estimation error for sensorless IPMSM drives, IEEE Trans. Power Electron. 38 (2) (2023) 1662–1671, http://dx.doi.org/10.1109/TPEL.2022.3214270.
[22] X. Wu, X. Yu, T. Wu, K. Lu, S. Huang, H. Cui, S. Fang, Complex-coefficient synchronous frequency filter-based position estimation error reduction for sensorless IPMSM drives, IEEE Trans. Power Electron. 37 (12) (2022) 15297–15307, http://dx.doi.org/10.1109/TPEL.2022.3193221.
[23] S. Lin, W. Zhang, An adaptive sliding-mode observer with a tangent function-based pll structure for position sensorless PMSM drives, Int. J. Electr. Power Energy Syst. 88 (2017) 63–74, http://dx.doi.org/10.1016/j.ijepes.2016.12.006.
[24] E. Ates, B. Tekgun, G. Ablay, Sensorless position and speed control of IPMSM with sliding mode observer and voltage signal injection, in: Proceedings - 2021 IEEE 3rd Global Power, Energy and Communication Conference, GPECOM 2021, IEEE, 2021, pp. 115–119, http://dx.doi.org/10.1109/GPECOM52585.2021.9587579, URL https://ieeexplore.ieee.org/stamp/stamp.jsp?arnumber=9587579.
[25] S. Dong, M. Zhou, X. You, C. Wang, A sensorless control strategy of injecting HF voltage into d-axis for IPMSM in full speed range, IEEE Trans. Power Electron. 37 (11) (2022) 13587–13597, http://dx.doi.org/10.1109/TPEL.2022.3183222.

[26] Y. Zhao, W. Qiao, L. Wu, An adaptive quasi-sliding-mode rotor position observer-based sensorless control for interior permanent magnet synchronous machines, IEEE Trans. Power Electron. 28 (12) (2013) 5618–5629, http://dx.doi.org/10.1109/TPEL.2013.2246871.

[27] J. Yoo, H.S. Kim, S.K. Sul, MTPA tracking control of sensorless IPMSM based on square-wave voltage signal injection, IEEE Trans. Power Electron. 37 (10) (2022) 12525–12537, http://dx.doi.org/10.1109/TPEL.2022.3179241.

[28] G. Wang, Z. Li, G. Zhang, Y. Yu, D. Xu, Quadrature PLL-based high-order sliding-mode observer for IPMSM sensorless control with online MTPA control strategy, IEEE Trans. Energy Convers. 28 (1) (2013) 214–224, http://dx.doi.org/10.1109/TEC.2012.2228484.

[29] K.H. Nam, AC motor control and electrical vehicle applications, 2019.